ACS APPLIED MATERIALS & INTERFACES

Research Article

www.acsami.org

Improved Hole-Transporting Property via HAT-CN for Perovskite Solar Cells without Lithium Salts

Yingzhuang Ma,[†] Yao-Hsien Chung,[†] Lingling Zheng,[†] Danfei Zhang,[†] Xiao Yu,[‡] Lixin Xiao,*[,†,§] Zhijian Chen,[†,§] Shufeng Wang,[†,§] Bo Qu,[†,§] Qihuang Gong,[†] and Dechun Zou*[,‡]

[†]State Key Laboratory for Mesoscopic Physics and Department of Physics, [‡]College of Chemistry and Molecular Engineering, Peking University, Beijing 100871, People's Republic of China

[§]New Display Device and System Integration Collaborative Innovation Center of the West Coast of the Taiwan Strait, Fuzhou 350002, People's Republic of China

Supporting Information

ABSTRACT: A nonadditive hole-transporting material (HTM) of a triphenylamine derivative of *N*,*N*′-di(3-methylphenyl)-*N*,*N*′-diphenyl-4,4′-diaminobiphenyl (TPD) is used for the organic−inorganic hybrid perovskite solar cells. The power conversion efficiency (PCE) can be significantly enhanced by inserting a thin layer of 1,4,5,8,9,11-hexaazatriphenylenehexacarbonitrile (HAT-CN) without adding an ion additive because the hole-transporting properties improve. The short-circuit current density (J_{sc}) increases from 8.5 to 13.1 mA/cm^2, the open-circuit voltage (V_{oc}) increases from 0.84 to 0.92 V, and the fill-factor (FF) increases from 0.45 to 0.59, which corresponds to the increase in PCE from 3.2% to 7.1%. Moreover, the PCE decreases by only 10% after approximately 1000 h without encapsulation, which suggests an alternative method to improve the stability of perovskite solar cells.

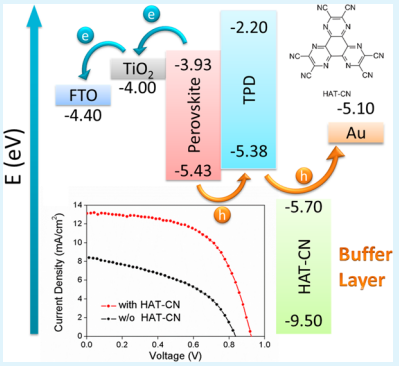

KEYWORDS: *interfacial, hole-transport, perovskite solar cell, HAT-CN, stability*

1. INTRODUCTION

Solar cells based on organic−inorganic hybrid perovskite have achieved over 15% of power conversion efficiencies (PCEs) shortly after the solidification of device because of its superior light absorption and outstanding charge-transporting properties.[1−6] Among these solid-state perovskite solar cells, the widely used hole-transporting material (HTM) of Spiro-MeOTAD (2,2′,7,7′-tetrakis(*N*,*N*-di-*p*-methoxyphenylamine)-9,9′-spirobifluorene) remains the highest performing material because of its long electron lifetime (suppressing recombination in the HTM layer) and well-matched HOMO (highest occupied molecular orbital) energy level to perovskite even with a low hole mobility of 10^{-5} cm^2 V^{-1} s^{-1}.[7] Although the conductivity can be enhanced by controlling the interface morphology, as shown in our previous report,[8] and doping with some ionic electrolytes, e.g., lithium bis-trifluoromethylsulfonyl amide (Li-TFSI), and Co(II) compounds,[9−13] the lithium salt readily absorbs humidity, which may lead to the decomposition of moisture-sensitive perovskite, shorten the operation time of the device, and prevent the commercialization of perovskite solar cells.[14,15]

In this work, we used a conventional triphenylamine derivative of *N*,*N*′-di(3-methylphenyl)-*N*,*N*′diphenyl-4,4′-diaminobiphenyl (TPD) as the HTM of perovskite solar cell, considering that TPD has a hole mobility as high as 10^{-3} cm^2 V^{-1} s^{-1} and a well-matched HOMO energy level (−5.38 eV) to perovskite (−5.43 eV), as shown in Figure 1. However, a low efficiency was obtained without adding an ion electrolyte. Therefore, a conventional buffer layer of 1,4,5,8,9,11-hexaazatriphenylenehexacarbonitrile (HAT-CN), which is widely used in semiconductor devices,[29−32] was inserted between TPD and the Au electrode. As a result, the photovoltaic performance was significantly improved. This approach indicates that an ion-electrolyte-free HTM can also effectively work in perovskite solar cells. Moreover, the resulting device has a long lifetime of 1000 h with only 10% degeneration, which suggests an alternative method to obtain perovskite solar cells with high stability.

2. EXPERIMENTAL SECTION

2.1. Materials. Hydroiodic acid (114 mmol, 15 mL, 57 wt %, Sigma-Aldrich, 99.99%) and methylamine (140 mmol, 70 mL, 2.0 M in methanol, Aldrich) were reacted at 0 °C with stirring in N_2 for 120 min. The resultant solution was evaporated to obtain a white precipitate, which was washed with diethyl ether several times until the diethyl ether was completely clear. The white precipitate was dried in a vacuum for 48 h and used without further purification. Other materials were used as received without purification.

2.2. Measurements. The absorption spectrum was recorded with a UV−visible spectrophotometer (Agilent 8453) using the sample without perovskite as the blank signal. The morphology measurement

Received: June 19, 2014
Accepted: March 11, 2015
Published: March 11, 2015

DOI: 10.1021/acsami.5b00149
ACS Appl. Mater. Interfaces 2015, 7, 6406−6411

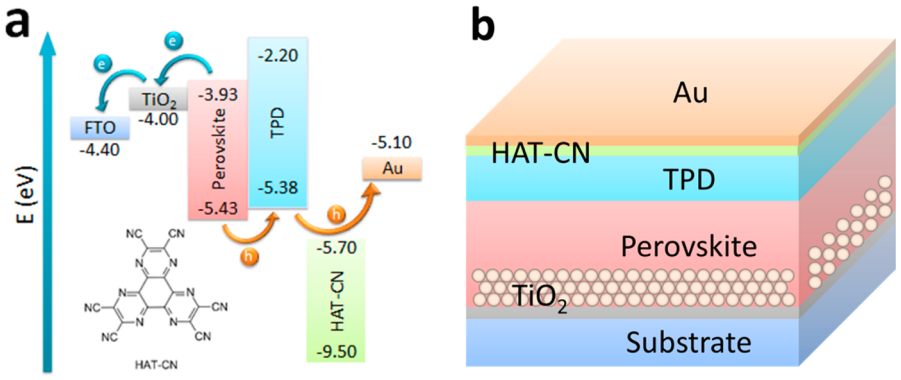

Figure 1. (a) Schematic illustration of the energy diagram with HAT-CN. (b) Structural illustration of device fabrication.

of the perovskite layers was performed using scanning electron microscopy (SEM, HITACHI 4300) and atomic force microscopy (AFM, Agilent Series 5500). Electrochemical impedance was performed using PGSTAT302N (Autolab Corp., Switzerland) at bias voltages of the open-circuit voltage. Photovoltaic performances were measured using a Keithley 2611 source meter under simulated sunlight from an Oriel 300 solar simulator according to the AM1.5G standard. The incident-photon-to-electron conversion efficiency (IPCE) was measured with a monochromator under 150 W halogen lamp (Crowntech, Qtest Station 2000). Both systems were calibrated against a certified reference solar cell. All measurements of the solar cells were performed with the active area of ~0.03 cm^2 in ambient atmosphere at room temperature without encapsulation. For the stability measurement, the device was stored in a box with humidity below 20%, without encapsulation, at room temperature and in the dark after the test.

2.3. Device Fabrication. Fluorine-doped tin oxide (FTO, Nippon Sheet Glass, 14 Ω/sq) glass was sequentially cleaned in water, acetone, and ethanol under ultrasonication for 15 min and subsequently treated with O_2 plasma for 15 min. The following procedure of compact the TiO_2 layer and mesoporous TiO_2 film followed our previous report.[16] To prepare the perovskite layer, a mixture of 0.5 M $PbCl_2$ (anhydrous, 99.99%, Alfa Aesar) and 0.5 M PbI_2 (anhydrous, 99.99%, Alfa Aesar) in *N*,*N*-dimethylformamide (anhydrous, 99.8%, Alfa Aesar) was spin-coated at 3000 rpm at 70 °C for 30 s and dried at 70 °C for 60 min. Then, the resulting film was dipped into a CH_3NH_3I solution (10 mg/mL in isopropyl alcohol) to form the perovskite crystalline and further dried at 70 °C for 30 min. To fabricate the device, 60 nm TPD (Nichem, Ni-H207) was coated using vacuum thermal deposition at an evaporation rate of 0.6 Å/s. For the device with HAT-CN, another 3 nm HAT-CN was deposited at an evaporation rate of 0.1 Å/s. Finally, 80 nm Au was thermally evaporated in a vacuum as the electrode.

3. RESULTS AND DISCUSSION

Figure 2 shows the cross section SEM image of the device with HAT-CN. The HAT-CN layer could not be identified from the image. The perovskite layer penetrated well into the mesoporous TiO_2 film and formed a continuous capping layer, which separates the HTM and the bare TiO_2. A high pore-filling fraction can sustain higher electron densities in the TiO_2 layer, which is beneficial to increase the electron-transporting rate, whereas the capping layer of perovskite is beneficial to suppress the charge recommendation between the HTM and TiO_2.[17]

Variations of the HAT-CN thickness were optimized using the thickness values of 1, 3, 5, and 10 nm. The data were supported by the statistical analysis from 15 devices. Figure 3 shows that the highest V_{oc} and FF values are at 3 nm, which

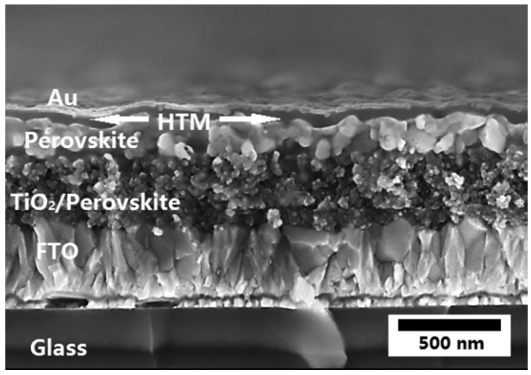

Figure 2. Cross section SEM image of the device.

leads to higher PCE for the devices, whereas J_{sc} does not show evident changes.

To further evaluate the morphology of the HTM layer, we measured the top morphology of the film with and without HTM as shown in Figure 4a,b, respectively. The perovskite capping layer mainly consisted of crystallites with an in-plane grain size of ~200 nm. According to the surface roughness, which was measured with AFM (Figure S1 of the Supporting Information), 60 nm of TPD was vacuum deposited to fully cover the perovskite layer; then, 3 nm HAT-CN was vacuum deposited. Figures 2 and 4 show that a compact TPD layer was formed on the perovskite layer, and the inset of Figure 4b shows that HAT-CN did not form a continuous film but spread as separated islands on the TPD layer.[28,29]

The device photovoltaic performances are shown in Figure 4 and listed in Table 1. The PCE of the device without HAT-CN was 3.2% with a short-circuit current (J_{sc}) of 8.5 mA/cm^2, open-circuit voltage (V_{oc}) of 0.84 V, and fill factor (FF) of 0.45. By inserting HAT-CN, the PCE was significantly increased to 7.1% with J_{sc} of 13.1 mA/cm^2, V_{oc} of 0.92 V, and FF of 0.59. The performances were simultaneously increased because of the presence of HAT-CN. The IPCEs are provided in Figure 5b, which is consistent with the absorption spectrum of the perovskite layer (see Figure S2 of the Supporting Information). The device with HAT-CN has higher IPCE values in the entire wavelength region. The integrated J_{sc} from the IPCE values were 8.7 and 13.3 mA/cm^2 for the devices without and with HAT-CN, respectively, which is consistent with the measured value.

It should be noted that the HAT-CN absorption is negligible compared to the perovskite layer (see Figure S2 of the Supporting Information). Considering the similar device

DOI: 10.1021/acsami.5b00149
ACS Appl. Mater. Interfaces 2015, 7, 6406−6411

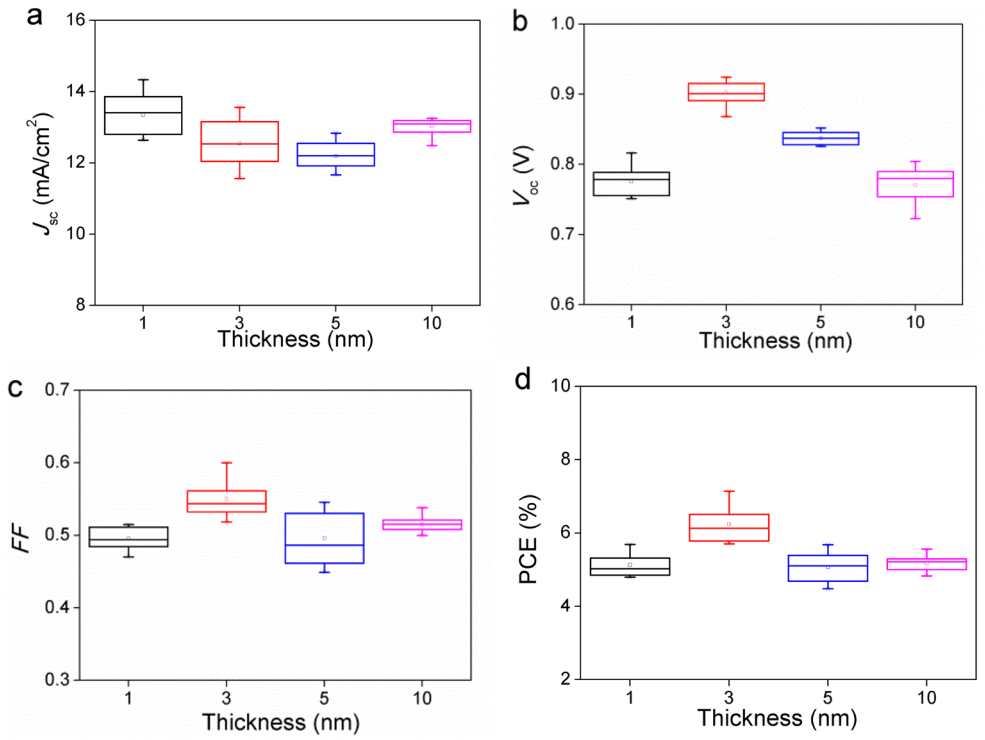

Figure 3. Optimization for device performance via variation of HAT-CN thickness. (a) J_{sc}, (b) V_{oc}, (c) FF, and (d) PCE.

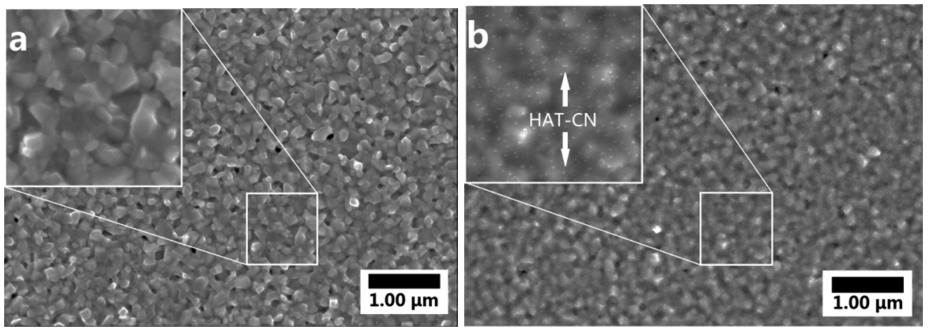

Figure 4. Top morphology of (a) FTO/TiO_2/perovskite and (b) FTO/TiO_2/perovskite/TPD/HAT-CN; the insets show the enlarged images.

Table 1. Role of HAT-CN in the Device Performance

device	J_{sc} (mA/cm^2)	V_{oc} (V)	FF	PCE (%)	R_s (Ω cm^2)	R_{sh} (Ω cm^2)
w/o HAT-CN	8.5	0.84	0.45	3.2	22	231
with HAT-CN	13.1	0.92	0.59	7.1	12	1062

configurations, it can be inferred that the PCE is mainly enhanced because the electronic properties improve, which is caused by HAT-CN. As listed in Table 1, the series resistance (R_s) could be obtained by linearly fitting from the $J-V$ curves around the point $J = 0$; the shunt resistance (R_{sh}) could be extracted around the point $V = 0$.[33] The device with HAT-CN has a R_s of 12 Ω cm^2 and a R_{sh} of 1062 Ω cm^2, whereas the device without HAT-CN has a larger R_s of 22 Ω cm^2 and a smaller R_{sh} of 231 Ω cm^2. Several factors may contribute to the higher performances of the device with HAT-CN compared to the device without HAT-CN. HAT-CN with deep LUMO (lowest unoccupied molecular orbital) level has been widely used as a hole-injection layer in OLED; then, the charge-transfer complex can be formed, by which several orders of magnitude increase in conductivity have been reported.[18−20] The LUMO of HAT-CN (−5.70 eV) is close to the HOMO of TPD (−5.38 eV); thus, the charge-transfer complex (dipole) at the TPD/HAT-CN interface readily forms to facilitate charge transport, which can reduce R_s and increases J_{sc}. The interfacial dipole layer at the TPD surface, which is formed by the HAT-CN insertion, may block the electron diffusion and improve the hole extraction, which reduces the recombination of charge carriers and results in a higher J_{sc}. The HAT-CN insertion can also decrease the Schottky barrier between the HTM of TPD and the Au electrode, which causes the energy level realignment and band bending to contribute to the increase in V_{oc}.[21] As a result, the electrical properties of the TPD/Au interface can be effectively modified by introducing HAT-CN, which significantly improves the device performances.

In perovskite solar cells, the HTM/TiO_2 and HTM/cathode are two types of recombination paths.[22,23] The electrochemical impedance can probe the interfacial redox processes between HTM and the electrode. In general, the low-frequency part of the impedance spectrum is related to the recombination at the

DOI: 10.1021/acsami.5b00149
ACS Appl. Mater. Interfaces 2015, 7, 6406−6411

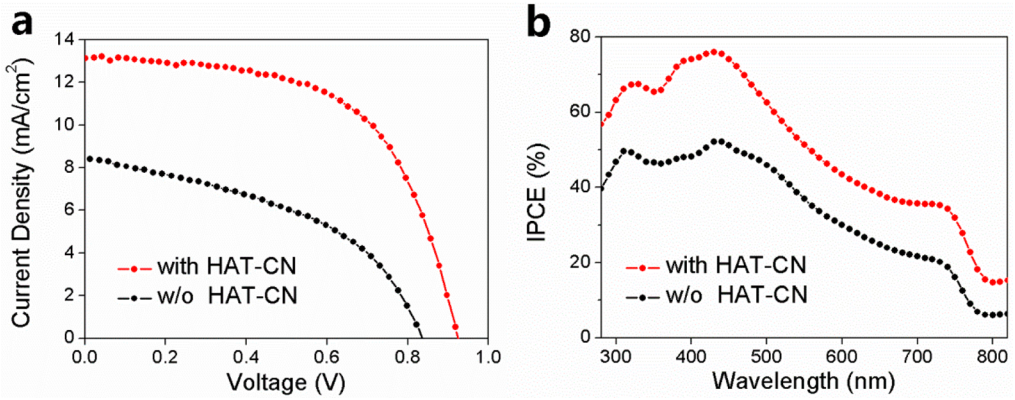

Figure 5. (a) Photovoltaic performance of device with (red curve) and without (black curve) HAT-CN. (b) IPCE of of device with (red curve) and without (black curve) HAT-CN.

interface between TiO_2 and HTM, and the high-frequency part may be attributed to the charge exchange process at the HTM/cathode interface and R_s.[24−26] The impedance was measured at a V_{oc} forward bias of −0.84 and −0.92 V for the device without and with HAT-CN, respectively. To analyze the impedance result, an R-C circuit model was used. R_1 represents the interfacial charge transfer resistance of the TPD/cathode. In Figure 6, the main arc represents the interface resistance of the

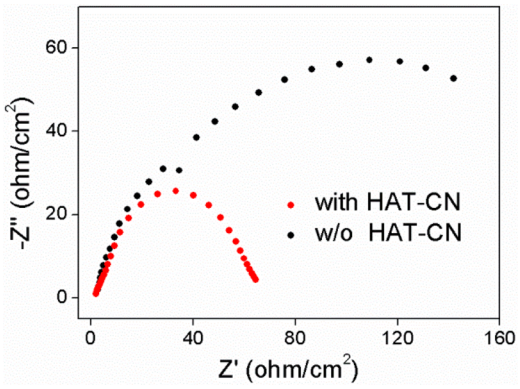

Figure 6. Nyquist plots of the device with (red curve) and without (black curve) HAT-CN.

TPD/cathode in the high-frequency region (see Bode plots, Figure S3 of the Supporting Information), and the semicircle of the device with HAT-CN (R_1 = 65 Ω cm^2) shows an obviously smaller impedance than the device without HAT-CN (R_1 = 220 Ω cm^2), which is consistent with the increase in FF.[27]

To further understand the effect of HAT-CN on the charge-transporting properties, we fabricated hole-only devices with structures of ITO/TPD/Au and ITO/TPD/HAT-CN/Au to evaluate the hole-transporting behaviors. The film thicknesses are strictly consistent with those in solar cell devices. The hole mobility was determined based on the space-charge-limited current (SCLC) model:[28]

$$J = \frac{9}{8}\varepsilon_r\varepsilon_0\mu_0\frac{V^2}{L^3} \quad (1)$$

where ε_0 is the dielectric permittivity of vacuum, ε_r is the relative permittivity, L is the thickness of the layer, and μ_0 is the zero-field mobility. The results are shown in Figure 7, and the device with HAT-CN exhibits an obviously higher hole mobility (3.5 × 10^{-5} cm^2 V^{-1} s^{-1} for the device with HAT-

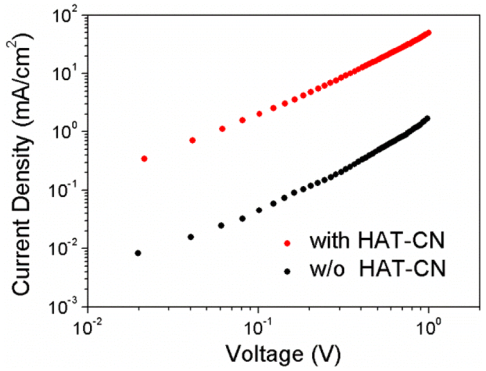

Figure 7. SCLC plot of hole-only device with (red curve) and without (black curve) HAT-CN.

CN and 1.9 × 10^{-6} cm^2 V^{-1} s^{-1} for the device without HAT-CN). This result is consistent with the aforementioned device performances, which can be ascribed to the improved hole-extraction ability and low charge injection barrier at the interface between TPD and the Au electrode.

As previously mentioned, the long-term stability is an important property for future commercialization. The device with HAT-CN showed considerable stability with humidity below 20% at room temperature without encapsulation in dark. As shown in Figure 8, V_{oc} remained stable with almost no decay, but J_{sc} showed a small overall decay with a small fluctuation. FF decreased with time from 0.59 to 0.52, which was the main reason for the decrease in PCE. The PCE decreased by only 10% after approximately 1000 h, which suggests an alternative method to obtain long stability for perovskite solar cells.

4. CONCLUSIONS

A conventional triphenylamine derivative of TPD was used as the HTM for organic−inorganic hybrid perovskite solar cells. The PCE can be significantly enhanced by inserting a thin layer of HAT-CN without adding ion additive. HAT-CN can decrease the injection barrier from TPD to the Au electrode, which decreases the V_{oc} loss across the interface of the heterojunction. HAT-CN can improve J_{sc} by forming the charge-transfer complex (dipole) between HTM and metal electrode, which is helpful for blocking electrons and extraction holes. Moreover, the PCE decreased by only 10% after approximately 1000 h without encapsulation because of the

DOI: 10.1021/acsami.5b00149
ACS Appl. Mater. Interfaces 2015, 7, 6406−6411

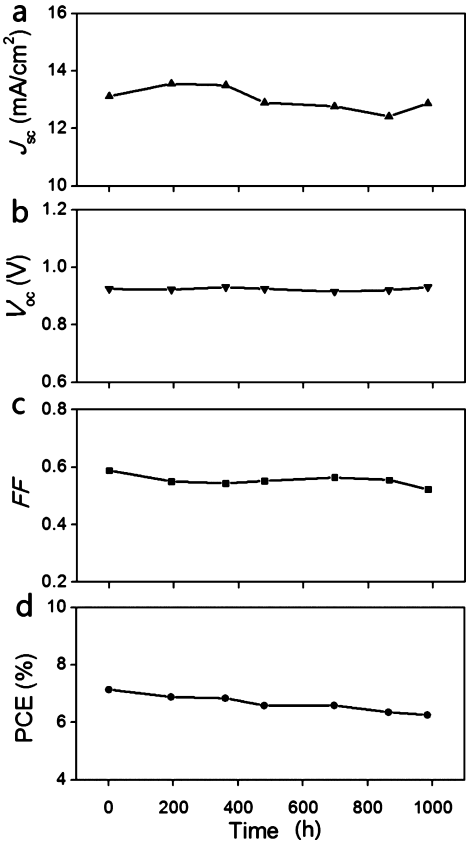

Figure 8. Stability test for device with HAT-CN. (a) J_{sc}, (b) V_{oc}, (c) FF, and (d) PCE.

absence of lithium salts, which prevented the absorbing of moisture. These results indicate an alternative method to improve the hole-transporting property of perovskite solar cells with long device stability.

■ ASSOCIATED CONTENT

Ⓢ Supporting Information

AFM image of the perovskite layer with the top view; absorption spectra of the perovskite/TPD layer with and without HAT-CN; the Bode plot of the impedance spectra; photovoltaic comparison of the devices with TPD and without TPD using only 3 nm HAT-CN; photovoltaic performance of the device with Spiro-OMeTAD. This material is available free of charge via the Internet at http://pubs.acs.org.

■ AUTHOR INFORMATION

Corresponding Authors

*L. Xiao. E-mail: lxxiao@pku.edu.cn.

*D. Zou. E-mail: dczou@pku.edu.cn.

Author Contributions

The paper was written with the contribution of all authors. All authors have given approval to the final version of the paper.

Notes

The authors declare no competing financial interest.

■ ACKNOWLEDGMENTS

This study was partly financially supported by the National Natural Science Foundation of China (61177020, 11121091) and the National Basic Research Program of China (2013CB328704).

■ REFERENCES

(1) Burschka, J.; Pellet, N.; Moon, S. J.; Humphry-Baker, R.; Gao, P.; Nazeeruddin, M. K.; Grätzel, M. Sequential Deposition as a Route to High-Performance Perovskite-Sensitized Solar Cells. *Nature* **2013**, *499*, 316−319.

(2) Liu, M.; Johnston, M. B.; Snaith, H. J. Efficient Planar Heterojunction Perovskite Solar Cells by Vapour Deposition. *Nature* **2013**, *501*, 395−398.

(3) Liu, D.; Kelly, T. L. Perovskite Solar Cells With A Planar Heterojunction Structure Prepared Using Room-Temperature Solution Processing Techniques. *Nat. Photonics* **2014**, *8*, 133−138.

(4) Wang, J. T.-W.; Ball, J. M.; Barea, E. M.; Abate, A.; Alexander-Webber, J. A.; Huang, J.; Saliba, M.; Mora-Sero, I.; Bisquert, J.; Snaith, H. J.; Nicholas, R. J. Low-Temperature Processed Electron Collection Layers of Graphene/TiO_2 Nanocomposites in Thin Film Perovskite Solar Cells. *Nano Lett.* **2014**, *14*, 724−730.

(5) Wojciechowski, K.; Saliba, M.; Leijtens, T.; Abate, A.; Snaith, H. J. Sub-150 °C Processed Meso-Superstructured Perovskite Solar Cells with Enhanced Efficiency. *Energy Environ. Sci.* **2014**, *7*, 1142−1147.

(6) Jeon, N. J.; Lee, H. J.; Kim, Y. C.; Seo, J.; Noh, J. H.; Lee, J.; Seok, S. I. *o*-Methoxy Substituents in Spiro-OMeTAD for Efficient Inorganic-Organic Hybrid Perovskite Solar Cells. *J. Am. Chem. Soc.* **2014**, *136*, 7837−7840.

(7) Bi, D.; Yang, L.; Boschloo, G.; Hagfeldt, A.; Johansson, E. M. J. Effect of Different Hole Transport Materials on Recombination in $CH_3NH_3PbI_3$ Perovskite-Sensitized Mesoscopic Solar Cells. *J. Phys. Chem. Lett.* **2013**, *4*, 1532−1536.

(8) Zheng, L.; Ma, Y.; Chu, S.; Wang, S.; Qu, B.; Xiao, L.; Chen, Z.; Gong, Q.; Wu, Z.; Hou, X. Improved Light Absorption and Charge Transport for Perovskite Solar Cells with Rough Interfaces by Sequential Deposition. *Nanoscale* **2014**, *6*, 8171−8176.

(9) Eperon, G. E.; Burlakov, V. M.; Docampo, P.; Goriely, A.; Snaith, H. J. Morphological Control for High Performance, Solution-Processed Planar Heterojunction Perovskite Solar Cells. *Adv. Funct. Mater.* **2014**, *24*, 151−157.

(10) Saliba, M.; Tan, K. W.; Sai, H.; Moore, D. T.; Scott, T.; Zhang, W.; Estroff, L. A.; Wiesner, U.; Snaith, H. J. Influence of Thermal Processing Protocol upon the Crystallization and Photovoltaic Performance of Organic−Inorganic Lead Trihalide Perovskites. *J. Phys. Chem. C* **2014**, *118*, 17171−17177.

(11) Dualeh, A.; Moehl, T.; Tétreault, N.; Teuscher, J.; Gao, P.; Nazeeruddin, M. K.; Grätzel, M. Impedance Spectroscopic Analysis of Lead Iodide Perovskite-Sensitized Solid-State Solar Cells. *ACS Nano* **2014**, *8*, 362−373.

(12) Burschka, J.; Kessler, F.; Nazeeruddin, M. K.; Grätzel, M. Co(III) Complexes as p-Dopants in Solid-State Dye-Sensitized Solar Cells. *Chem. Mater.* **2013**, *25*, 2986−2990.

(13) Zhang, H.; Shi, Y.; Yan, F.; Wang, L.; Wang, K.; Xing, Y.; Dong, Q.; Ma, T. A Dual Functional Additive for the HTM Layer in Perovskite Solar Cells. *Chem. Commun.* **2014**, *50*, 5020−5022.

(14) Noh, J. H.; Im, S. H.; Heo, J. H.; Mandal, T. N.; Seok, S. I. Chemical Management for Colorful, Efficient, and Stable Inorganic-Organic Hybrid Nanostructured Solar Cells. *Nano Lett.* **2013**, *13*, 1764−1769.

(15) Zheng, L.; Chung, Y.-H.; Ma, Y.; Zhang, L.; Xiao, L.; Chen, Z.; Wang, S.; Qu, B.; Gong, Q. A Hydrophobic Hole Transporting Oligothiophene for Planar Perovskite Solar Cells with Improved Stability. *Chem. Commun.* **2014**, *50*, 11196−11199.

(16) Ma, Y.; Zheng, L.; Chung, Y.-H.; Chu, S.; Xiao, L.; Chen, Z.; Wang, S.; Qu, B.; Gong, Q.; Wu, Z.; Hou, X. A Highly Efficient Mesoscopic Solar Cell Based on $CH_3NH_3PbI_{3-x}Cl_x$ Fabricated *via* Sequential Solution Deposition. *Chem. Commun.* **2014**, *50*, 12458−12461.

(17) Leijtens, T.; Lauber, B.; Eperon, G. E.; Stranks, S. D.; Snaith, H. J. The Importance of Perovskite Pore Filling in Organometal Mixed Halide Sensitized TiO_2-based Solar Cells. *J. Phys. Chem. Lett.* **2014**, *5*, 1096−1102.

(18) Kim, Y.-K.; Kim, J. W.; Park, Y. Energy Level Alignment at a Charge Generation Interface Between 4,4-Bis(*N*-phenyl-1-

DOI: 10.1021/acsami.5b00149
ACS Appl. Mater. Interfaces 2015, 7, 6406−6411

naphthylamino)biphenyl and 1,4,5,8,9,11-Hexaazatriphenylene-hexacarbonitrile. *Appl. Phys. Lett.* **2009**, *94*, 063305−063307.
(19) Park, S. M.; Kim, Y. H.; Yi, Y.; Oh, H.-Y.; Kim, J. W. Insertion of an Organic Interlayer for Hole Current Enhancement in Inverted Organic Light Emitting Devices. *Appl. Phys. Lett.* **2010**, *97*, 063308−063310.
(20) Lee, J.-H.; Lee, S.; Kim, J.-B.; Jang, J.; Kim, J. J. A High Performance Transparent Inverted Organic Light Emitting Diode with 1,4,5,8,9,11-Hexaazatriphenylenehexacarbonitrile as an Organic Buffer Layer. *J. Mater. Chem.* **2012**, *22*, 15262−15266.
(21) Luo, J.; Xiao, L.; Chen, Z.; Qu, B.; Gong, Q. Insulator MnO: Highly Efficient and Air-stable n-type Doping Layer for Organic Photovoltaic Cells. *Org. Electron.* **2010**, *11*, 664−669.
(22) Gonzalez-Pedro, V.; Juarez-Perez, E. J.; Arsyad, W.-S.; Barea, E. M.; Fabregat-Santiago, F.; Mora-Sero, I.; Bisquert, J. General Working Principles of $CH_3NH_3PbX_3$ Perovskite Solar Cells. *Nano Lett.* **2014**, *14*, 888−893.
(23) Juarez-Perez, E. J.; Wuβler, M.; Fabregat-Santiago, F.; Lakus-Wollny, K.; Mankel, E.; Mayer, T.; Jaegermann, W.; Mora-Sero, I. Role of the Selective Contacts in the Performance of Lead Halide Perovskite Solar Cells. *J. Phys. Chem. Lett.* **2014**, *5*, 680−685.
(24) Wang, Q.; Moser, J.-E.; Grätzel, M. Electrochemical Impedance Spectroscopic Analysis of Dye-Sensitized Solar Cells. *J. Phys. Chem. B* **2005**, *109*, 14945−14953.
(25) Fabregat-Santiago, F.; Bisquert, J.; Cevey, L.; Chen, P.; Wang, M.; Zakeeruddin, S. M.; Grätzel, M. Electron Transport and Recombination in Solid-State Dye Solar Cell with Spiro-OMeTAD as Hole Conductor. *J. Am. Chem. Soc.* **2009**, *131*, 558−562.
(26) Fabregat-Santiago, F.; Bisquert, J.; Palomares, E.; Otero, L.; Kuang, D.; Zakeeruddin, S. M.; Grätzel, M. Correlation between Photovoltaic Performance and Impedance Spectroscopy of Dye-Sensitized Solar Cells Based on Ionic Liquids. *J. Phys. Chem. C* **2007**, *111*, 6550−6560.
(27) Wang, M.; Moon, S. J.; Zhou, D.; Le Formal, F.; Cevey-Ha, N. L.; Humphry-Baker, R.; Grätzel, C.; Wang, P.; Zakeeruddin, S. M.; Grätzel, M. Enhanced-Light-Harvesting Amphiphilic Ruthenium Dye for Efficient Solid-State Dye-Sensitized Solar Cells. *Adv. Funct. Mater.* **2010**, *20*, 1821−1826.
(28) Zhang, L.; Xing, X.; Chen, Z.; Xiao, L.; Qu, B.; Gong, Q. Highly Efficient Polymer Solar Cells by using the Homogeneous Self-Assembly of a Sulphydryl-Capped Photoactive Polymer Covalently Bound to the Anode. *Energy Technol.* **2013**, *1*, 613−616.
(29) Saragi, T. P.; Reichert, T.; Scheffler, A.; Kussler, M.; Salbeck, J. Electron Mobility in Hexaazatriphenylene Hexacarbonitrile Field-Effect Transistors. *Synth. Met.* **2012**, *162*, 1572−1576.
(30) Lin, H. W.; Lin, W. C.; Chang, J. H.; Wu, C. I. Solution-Processed Hexaazatriphenylene Hexacarbonitrile as a Universal Hole-Injection Layer for Organic Light-Emitting Diodes. *Org. Electron.* **2013**, *14*, 1204−1210.
(31) Kim, D. H.; Kim, T. W. Efficiency Enhancement in Tandem Organic Light-Emitting Devices with a Hybrid Charge Generation Layer Composed of BEDT-TTF-Doped TPBi/mCP/HAT-CN. *Org. Electron.* **2014**, *15*, 3452−3457.
(32) Jeon, S. O.; Lee, J. Y. Improved Efficiency of Inverted Organic Solar Cells Using Organic Hole Collecting Interlayer. *J. Ind. Eng. Chem.* **2012**, *18*, 661−663.
(33) Aernouts, T.; Geens, W.; Poortmans, J.; Heremans, P.; Borghs, S.; Mertens, R. Extraction of Bulk and Contact Components of the Series Resistance in Organic Bulk Donor-Acceptor-Heterojunctions. *Thin Solid Films* **2002**, *403*, 297−301.

DOI: 10.1021/acsami.5b00149
ACS Appl. Mater. Interfaces 2015, 7, 6406−6411